Available online at www.sciencedirect.com
SCIENCE DIRECT®
Archives of Biochemistry and Biophysics 442 (2005) 169–179
ABB
www.elsevier.com/locate/yabbi

# Structural and mutational studies of organophosphorus hydrolase reveal a cryptic and functional allosteric-binding site ☆,☆☆

Janet K. Grimsley [a], Barbara Calamini [b], James R. Wild [a,*], Andrew D. Mesecar [b,*]

[a] *Biochemistry and Biophysics Department, Texas A&M University, College Station, TX 77843-2128, USA*
[b] *University of Illinois at Chicago, Department of Medicinal Chemistry and Pharmacognosy and the Center for Pharmaceutical Biotechnology, Chicago, IL 60607, USA*

Received 22 June 2005, and in revised form 4 August 2005
Available online 6 September 2005

**Abstract**

Organophosphorus hydrolase detoxifies a broad range of organophosphate pesticides and the chemical warfare agents (CWAs) sarin and VX. Previously, rational genetic engineering produced OPH variants with 30-fold enhancements in the hydrolysis of CWA and their analogs. One interesting variant (H254R) in which the histidine at position 254 was changed to an arginine showed a 4-fold increase in the hydrolysis of demetonS (VX analog), a 14-fold decrease with paraoxon (an insecticide), and a 183-fold decrease with DFP (sarin analog). The three-dimensional structure of this enzyme at 1.9 Å resolution with the inhibitor, diethyl 4-methylbenzylphosphonate (EBP), revealed that the inhibitor did not bind at the active site, but bound exclusively into a well-defined surface pocket 12 A away from the active site. This structural feature was accompanied by non-competitive inhibition of paraoxon hydrolysis by EBP with H254R, in contrast to the native enzyme, which showed competitive inhibition. These parallel structure–function characteristics identify a functional, allosteric site on the surface of this enzyme.


*Keywords:* Phosphotriesterase; Allostery; Non-competitive inhibition; Chemical warfare agents; X-ray crystallography; Allosteric site; Competitive inhibition

Organophosphorus hydrolase (OPH; EC 3.1.8.1)[1] is a dimeric, binuclear metalloenzyme isolated from the soil bacterium *Pseudomonas diminuta* [1–3] that detoxifies many organophosphate pesticides and related chemical warfare agents (CWAs). Rate enhancements by OPH approach the diffusion-controlled limit with the enzyme's best substrate, paraoxon, which undergoes P–O bond cleavage [4]. However, the substrate specificities for CWAs are much lower ($k_{cat}/K_M \sim 1$–$8.0 \times 10^4\ M^{-1}\ s^{-1}$). These enzymatic transformations are interesting since there are very few naturally occurring organophosphate triesters. In fact, the native function of OPH still remains unknown. Nonetheless, OPH is of considerable interest for use in commercial applications for detoxification of agricultural insecticides and chemical warfare nerve agents. OPH is the only enzyme known that is capable of hydrolyzing the P–S bond of phosphonothioate esters [5,6]. However, the rates of hydrolysis ($k_{cat} \sim 0.30\ s^{-1}$) for this class of compounds, which includes the V chemical warfare agents, VX and RVX [7,8], are much slower than the hydrolytic rates for many of the phosphotriester compounds such as sarin and tabun ($k_{cat} = 56$ and $77\ s^{-1}$, respectively) [6,9].

☆ This work was supported in part by a grant from the US Army Medical Research and Materiel Command (Cooperative Agreement #DAMD 17-00-2-0010), the National Science Foundation (Grant MCB9904635), and the Robert A. Welch Foundation (#931). The contributions of A.D.M. and B.C. were made in part through grant support from the Office of Naval Research (N000140210956) and NIH-NIGMS (1 R01 GM072357-01).
☆☆ X-ray coordinates have been deposited in the Research Collaboratory for Structural Bioinformatics, Rutgers University, New Brunswick, NJ (1QW7).
* Corresponding authors. Fax: +1 979 845 9274 (J.R. Wild), fax: +1 312 413 9303 (A.D. Mesecar).
*E-mail addresses:* j-wild@tamu.edu (J.R. Wild), mesecar@uic.edu (A.D. Mesecar).
[1] *Abbreviations used:* OPH, organophosphorus hydrolase; CWAs, chemical warfare agents; EBP, diethyl 4-methylbenzylphosphonate; OPDA, organophosphate-degrading enzyme; PTP1B, protein tyrosine phosphatase 1B; GPb, glycogen phosphorylase b.

0003-9861/$ - see front matter © 2005 Elsevier Inc. All rights reserved.
doi:10.1016/j.abb.2005.08.012

X-ray crystallographic studies [10–12] have verified that OPH is a dimeric metalloenzyme that contains two equivalents of zinc per monomer. Each monomer is an α/β barrel with eight strands of a parallel β-pleated sheet (TIM barrel). Each active site has a binuclear metal center and several metals ($Co^{2+}$, $Cd^{2+}$, $Ni^{2+}$, $Mn^{2+}$, or $Fe^{2+}$) can substitute for the native zinc with varying affects on rates of hydrolysis [13]. When paraoxon is used as the substrate, turnover numbers range from 10,000 $s^{-1}$ for WT-$Co^{2+}$ to 100 $s^{-1}$ for the $Fe^{2+}$-liganded enzyme. The $Co^{2+}$ form of the enzyme is also the most active with sarin, soman, and VX [6].

Fig. 1 represents the proposed model for the initial catalytic complex in which the phosphoryl–oxygen bond of the substrate is polarized through its association with the more solvent exposed metal (M2) in the active site [14]. Nucleophilic attack on the substrate occurs from the water molecule or hydroxide ion that bridges the two metal ions. This water or hydroxide is also hydrogen bonded to the carboxylate of Asp301. The catalytic mechanism would then proceed via a $S_N2$ process in which the activated water molecule attacks the phosphoryl center of the substrate, resulting in the displacement of the leaving group with an inversion of stereochemical configuration [15]. The arrows in Fig. 1 represent the flow of electrons from the activated water molecule to the displacement of the leaving group of the substrate.

Site-directed mutations of histidines near the OPH active site resulted in three OPH variants with a 4- to 30-fold increase in substrate specificity and enhanced rates of hydrolysis for demeton-S (P–S bond) and NPPMP (P–O bond), analogs for the chemical warfare agents VX and soman, respectively [16]. Substitution of the histidine at position 254 with an arginine resulted in a 4- to 5-fold increase in the turnover number ($k_{cat}$) and the substrate specificity ($k_{cat}/K_M$) for demeton-S. However, this rate increase was compromised by a 12-fold decrease in the turnover number for paraoxon (P–O bond hydrolysis). Other studies suggested that substitution of the histidine at position 254 affected the kinetic characteristics of some substrates without affecting paraoxon hydrolysis [17–19]. The characterization of P–S bond hydrolysis by OPH indicated that demeton-S was a non-competitive inhibitor against paraoxon hydrolysis [20], yet mipafox, which contains a P–F bond, was shown to be a competitive inhibitor [5]. These results suggested at least one of the binding sites or binding orientations for demetonS was not identical to that for paraoxon.

This report describes the determination of the three-dimensional structure of the $Co^{2+}$-liganded, H254R enzyme in complex with diethyl 4-methylbenzylphosphonate (EBP). This is the first X-ray structure of *P. diminuta* OPH that has been determined with $Co^{2+}$ as the active-site metal. The combined catalytic and structural data for H254R identified a cryptic allosteric site that is able to influence the catalytic activity of *P. diminuta* OPH heterotropically via a non-competitive mechanism. A structural model is presented that explains the unique kinetics associated with the H254R enzyme.

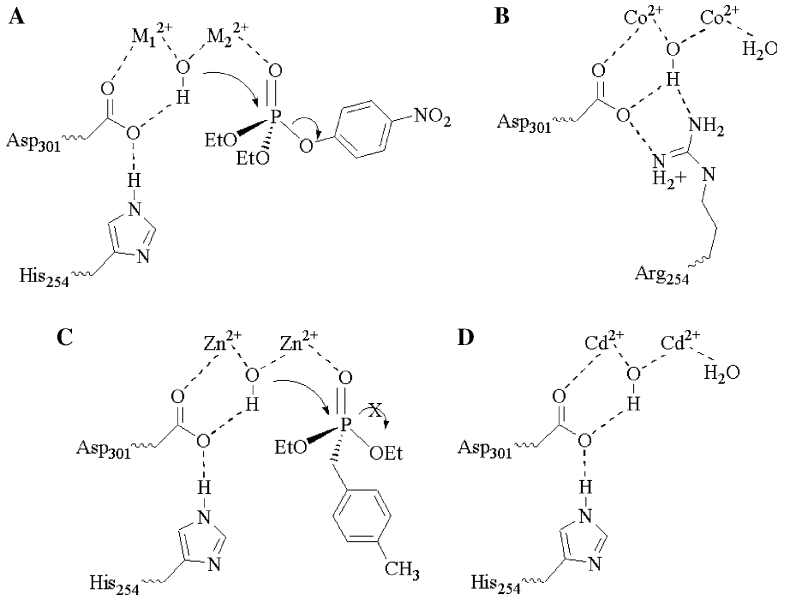


Fig. 1. Schematic diagrams of the active-site structures for various *P. diminuta* OPH enzymes. (A) The general active-site structure and mechanism for the OPH-catalyzed hydrolysis of the substrate paraoxon. The leaving group *p*-nitrophenol is shown in the proper orientation for a $S_N2$ mechanism. The highest activity of OPH is achieved when $M_1$ and $M_2$ are $Co^{2+}$, followed by $Ni^{2+}$, $Cd^{2+}$, $Zn^{2+}$, and $Mn^{2+}$ [13]. (B) X-ray structure of $Co^{2+}$-substituted H254R determined in this study. The inhibitor EBP was not observed in the active site but is observed in the allosteric site. (C) X-ray structure of wild-type, $Zn^{2+}$-substituted OPH [12] with EBP bound in both the active and allosteric sites. Note that the 4-methylbenzyl group that would be analogous to the 4-nitrophenol leaving group in paraoxon is in the wrong orientation for an $S_N2$ mechanism. (D) X-ray structure of wild-type, $Cd^{2+}$-substituted OPH [11] with EBP bound in only the allosteric site.

## Experimental procedures

### *Neurotoxic substrates and analogs*

Paraoxon was obtained from ChemService (Westchester, PA). The paraoxon is fully dispersed and dissolved in $ddH_2O$ and the final concentration was determined using the extinction coefficient of 8900 $M^{-1}$ $cm^{-1}$ at 274 nm. The paraoxon solution was stored at 4 °C. The non-hydrolyzable substrate analog, EBP, was purchased from Acros Organics (Morris Plains, NJ). EBP is fully dispersed and dissolved in 20 mM CHES, pH 9, and stored at 4 °C.

### *Purification and crystallization procedures*

The H254R enzyme was purified as described previously [21]. Cobalt chloride at a concentration of 1 mM was added to the growth media in order to produce the cobalt-bound form of the H254R enzyme in vivo. Immediately following purification of the cobalt-incorporated enzyme, it was concentrated in 10 mM TRIZMA, pH 8.3, to a final concentration of 11 mg/ml, followed by repeated washes in the same buffer. The concentrated enzyme was stored at 4 °C and used within 24 h. The protein was diluted to 5.8 mg/ml with 20 mM HEPES, pH 7.5. Single crystals of cobalt-incorporated H254R were grown by the hanging drop method [22] at room temperature. The crystallization solution contained 9% PEG 6000, 100 mM CHES, pH 9.0, 1% EBP, and 5 mM sodium azide. No additional cobalt was added to the crystallization solution.

### *X-ray data collection*

H254R crystals containing 1% EBP were serially transferred to cryoprotectant solutions of a synthetic mother-liquor (see above) containing 6, 12, 18, and 23% ethylene glycol. The crystal was then flash-cooled to 100 K in a stream of nitrogen gas for data collection. X-ray data were collected from a single crystal using an ADSC Q4 CCD detector at Beamline 5.02 at the Advanced Light Source. X-ray data were collected to a resolution of 1.9 Å and were processed and scaled using the programs DENZO and SCALEPACK [23]. The H254R–$Co^{2+}$–EBP complex crystallized in space group C2 with unit cell dimensions $a = 126.72$ Å, $b = 89.88$ Å, $c = 68.34$ Å, $\beta = 91.73°$. A summary of the relevant X-ray data collection statistics is presented in Table 1.

### *X-ray structure refinement*

The initial phases for H254R were determined by the method of molecular replacement using the program evolutionary programming molecular replacement (EPMR) [24]. The search model used for molecular replacement consisted of the dimer of wild-type OPH from *P. diminuta* (PDB: 1DPM) [11] with all side chains intact and ligands removed. The final and optimal molecular replacement solution contained a single dimer in the asymmetric unit and had a correlation coefficient greater than 0.6 using a resolution range of 20–3 Å. Iterative rounds of positional and B-factor refinement were performed with crystallography and NMR system (CNS) using a maximum likelihood target function and no sigma cutoff on structure factor amplitudes [25]. SigmaA, FOM-weighted electron density maps were created in CNS, and manual rebuilding was performed with the program O [26]. After three rounds of initial refinement, we were able to observe in difference fourier density maps, electron density for five additional amino acid residues on the N-terminus (Ser30-Ile31-Gly32-Thr33-Gly34-) and two more residues on the C-terminus (-Ala364-Ser365-) that were previously unobserved in *P. diminuta* X-ray structures even at 1.3 Å [27]. In addition, the initial electron density difference maps clearly indicated in each monomer the His254 to Arg254 mutation, two cobalt atoms in the active site, and a single molecule of EBP bound in an ancillary or allosteric site, but not the active

Table 1
Data collection and refinement statistics for *P. diminuta* H254R

| | |
|---|---|
| *Data collection parameters* | |
| Crystal conditions | Flash-cooled at 100 K |
| X-ray source | ALS Beamline 5.0.2 |
| Wavelength (Å) | 1.15 |
| Resolution limit (Å) | 1.90 |
| Space group | C121 |
| Cell dimensions | $a = 126.72$ Å, $b = 89.88$ Å, $c = 68.34$ Å, $\beta = 91.73°$ |
| *Data processing statistics* | *Overall [last shell]* |
| Data resolution range (Å) | 49.5–1.90 Å [1.97–1.90] |
| Reflections | |
| Total measured | 349,195 |
| Unique measured | 48,009 |
| Completeness (%) | 79.4 [43.6] |
| Average redundancy | 7.3 |
| $R_{merge}$ (%) | 11.5 [24.4] |
| Average $I/\sigma I$ | 10.4 [3.2] |
| *Refinement statistics* | *Overall [last shell]* |
| Data resolution range (Å) | 49.5–1.90 Å [1.97–1.90] |
| $R_{cryst}$ (%) | 17.8 [34.3] |
| $R_{free}$ (%) | 22.9 [29.9] |
| RMS deviations | |
| Bond length (Å) | 0.013 |
| Bond angles (°) | 1.7 |
| Dihedrals (°) | 22.7 |
| Impropers (°) | 1.03 |
| ESD from Luzzati plot (Å) | 0.21 |
| *Molecules in final model (#)* | *Average B-factor [Chain A, Chain B] (Å²)* |
| Protein (2) | Wilson Plot = 15.5 (Å²) |
| | Mean *B*-value = 26.5 (Å²) |
| EBP (2) | [30.4, 35.6] |
| $Co^{2+}$ (2) | [13.1, 13.9] |
| $Na^{+}$ (2) | [41.1, 41.1] |
| Solvent $H_2O$ (525) | NA |
| *Alternate sidechain Conformations (#)* | *Average B-factor [Conformation 1, Conformation 2] (Å²)* |
| Phe 132 (2) | Chain A [24.7, 20.6] |
| | Chain B [19.9, 27.5] |
| Thr173 (2) | Chain A [25.5, 27.0] |
| | Chain B [35.7, 36.5] |

site. Therefore, these additional amino acid residues, the two cobalt atoms, and EBP were added, the H254R substitution was made, and all atoms were manually modeled into the difference electron density. Iterative rounds of refinement were performed, and water molecules were added manually into strong (+ 4 σ) difference density peaks in the initial refinement stages, and into peaks of (+ 3 σ) in the final stages of refinement. During these iterative refinement rounds, it was clear that two amino acid residues in the active site (Phe132 and Thr173) each occupied two alternate conformations. We set the occupancies at 50% for each alternate conformation and continued refinement until the $R_{cryst}$ and $R_{free}$ values plateaued at their lowest values, which were 17.8 and 22.9% overall to 1.9 Å. These values compare well to the best $R_{cryst}$ and $R_{free}$ values of 19.1 and 22.8% that were reported for 1.3 Å structures of wild-type *P. diminuta* OPH [27]. The final model was validated using Procheck, MolProbity, and WhatCheck [28–30]. The final model coordinates were deposited in the Protein Data Bank [31] under PDB# 1QW7.

### *Docking methods*

Automated docking was conducted with DOCK (version 4.0) [32]. The following Brookhaven database entries were used: 1DPM, the zinc-containing *P. diminuta* OPH in complex with EBP which is bound in the active site and on the surface of the protein [12]; and 1QW7, H254R *P. diminuta* OPH with EBP bound only in an ancillary site. The same procedures were applied to both proteins, unless otherwise specified. The crystallographic water molecules were removed from the active site before docking calculations were performed with the exception of one metal-bound water molecule, which is important for catalysis. The two zinc atoms in 1DPM were converted to cobalt using the program SYBYL (version 6.6, Tripos, St. Louis, MO). The metal ions were left in the active site during docking. The SYBYL program package was also used to generate missing hydrogen atoms for the protein and the ligand. The partial charges for the protein atoms were taken from the AMBER force field [33,34]. The 1DPM structure was superimposed onto H254R in order to assign new coordinates to the EBP before the docking calculation in the H254R active site. The protein molecular surface was calculated using the program MS [35]. This surface served as input for the SPHGEN module of DOCK 4.0, which generates overlapping spheres that fill the protein active site. The SPHGEN output was analyzed in order to remove redundant spheres. A cluster of 88 and 31 spheres were used in 1DPM and 1QW7, respectively. The created clusters were enclosed in a box, and force fields scoring grids were generated by the GRID module of DOCK 4.0. The ligand EBP was docked by optimizing overlap with the active-site spheres and computing interaction energies with the grids. The maximum number or orientations of the ligand was limited to 5000, and only the 50 lowest solutions were saved and evaluated.

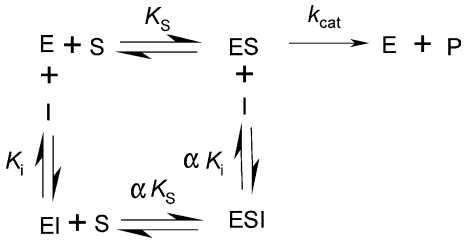


Scheme 1.

### *Kinetic characterization*

Catalytic rates ($k_{cat}$), the Michaelis constant ($K_M$), the inhibition constants ($K_{is}$) for paraoxon, and the $K_i$ for EBP were determined by performing enzymatic assays on changing concentrations of substrate with a constant concentration of enzyme. Substrate hydrolysis of paraoxon yielded *p*-nitrophenol as a hydrolytic cleavage product, and assays were monitored by following the appearance of the product ($\varepsilon_{400} = 17{,}000\ M^{-1}\ cm^{-1}$) in a reaction mixture containing 20 mM CHES at pH 9.0 and 25 °C. Assays were initiated by the addition of paraoxon. The concentration of EBP used in the inhibition assays ranged from 0.025 to 6.4 mM and was added to the reaction mixture immediately prior to initiation. Substrate concentration versus velocity curves were fit using the Enzyme Kinetics Module, version 1.1, from Sigma Plot, SPSS (Chicago, IL). The kinetic parameters $k_{cat}$, $K_M$, $K_i$, $K_{is}$, and α were determined directly from these applied curve fits. Data for both enzymes without added inhibitor were fit to either the Michaelis–Menten equation or to the following equation for substrate inhibition: $v = V_{max}/(1 + I/K_{is} + K_M/S)$. The data for the enzymes with added inhibitor were fit to the following equations for competitive inhibition (Eq. (1)) or linear mixed-type inhibition (Eq. (2)).

$$v = V_{max}/(1 + (K_M/S)(1 + I/K_i)), \quad (1)$$

$$v = V_{max}/((K_M/S)(1 + I/K_i) + (1 + I/(\alpha K_i))). \quad (2)$$

The factor α in Eq. (2) accounts for the amount by which the dissociation constants for $S$ ($K_S$) and $I$ ($K_i$) change when inhibitor or substrate occupied the enzyme, respectively [36]. The equilibria describing this system are shown in Scheme 1.

## Results

### *H254R active site*

The electron density around the metals in the active site of H254R is shown in Fig. 2A. Two cobalt ions are present in each active site of the dimer in the asymmetric unit, and the bridging ligands for the binuclear metal center are a hydroxide ion and Lys169, which is carbamylated (Lyx169) as observed in the $Cd^{2+}$- and $Zn^{2+}$-containing enzymes [11,12]. Electron density associated with EBP is absent in the active site of H254R. However, several water

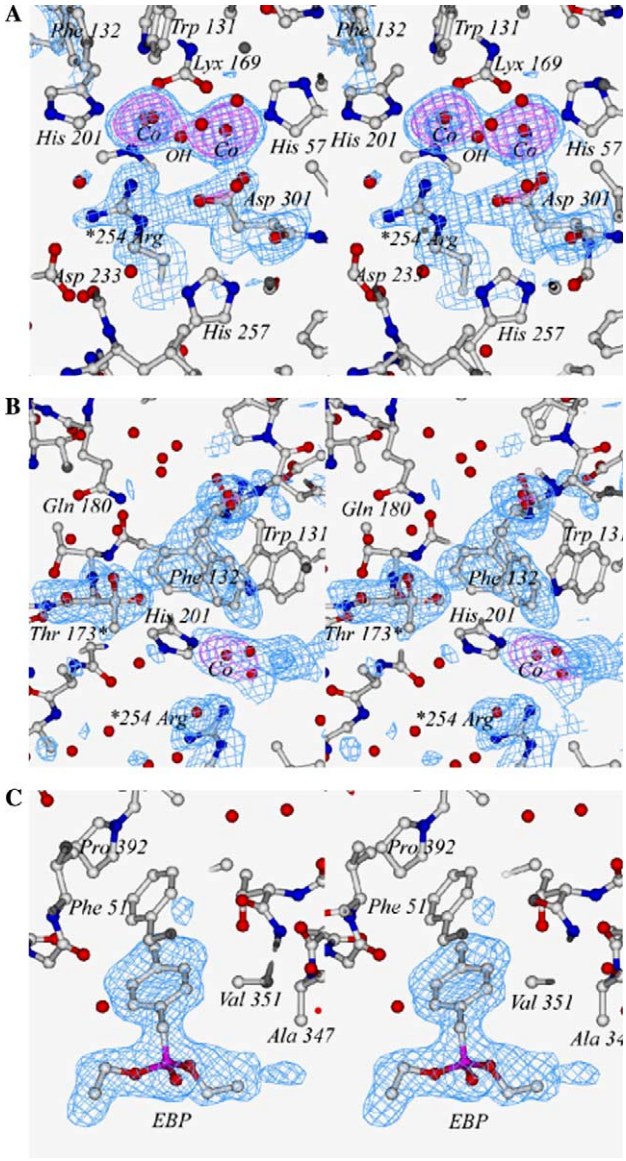


Fig. 2. Stereoviews of the final electron density ($F_o - F_c$) omit maps in the active site (A,B) and ancillary site (C) of H254R. The electron density is contoured at 3$\sigma$ (blue) and 10$\sigma$ (purple), and the two cobalt atoms, Arg254, Asp301, Thr301, Phe137, and EBP were omitted from the Difference-Fourier calculations. Red balls represent water molecules. The catalytic hydroxide is labeled as OH. The substitution at position 254 with arginine is indicated with an asterisk. The figures were made using SPOCK [53]. (For interpretation of the references to color in this figure legend, the reader is referred to the web version of this paper.)

molecules were observed in its place. In addition, one new water molecule is located within 3 Å of the guanidinium group of Arg254 in the active sites of both monomers of the dimer in the asymmetric unit. The only other significant differences within the active site were the positions of Phe132 and Thr173. These two residues have two different conformations in each of the subunits of the H254R dimer (Fig. 2B). Interestingly, these residues are not observed to have multiple conformations in the high-resolution (1.3 Å) structures of the native enzyme complexes with $Zn^{2+}$, $Cd^{2+}$ or $Mn^{2+}$ [27]. These structures have over 15

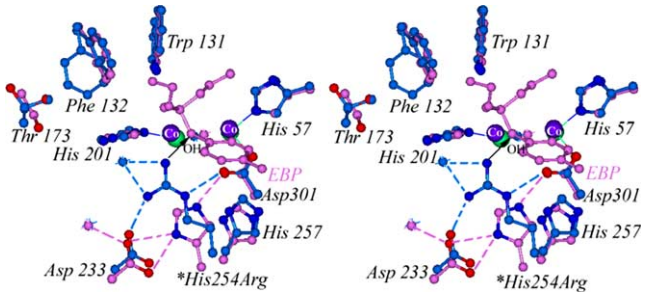


Fig. 3. Stereoviews of the superposition of the $Co^{2+}$-H254R active site (blue) with that of the $Zn^{2+}$-OPH active site (purple) that includes EBP (1DPM). Water molecules are colored accordingly. The $Co^{2+}$ ions from H254R are labeled, and the large green balls represent the wild-type $Zn^{2+}$ ions. Note the similarities in the hydrogen-bonded network within each active site (dashed lines) and the additional water molecule associated with the substituted arginine. The black arrow represents the steric overlap that would result from the overlap of the nitrogen of Arg254 and EBP. The figure was made using InsightII from Accelrys. (For interpretation of the references to color in this figure legend, the reader is referred to the web version of this paper.)

residues modeled in alternate conformations yet Phe132 and Thr173 are not among them.

The superposition of the $Co^{2+}$-containing, H254R active-site structure with the $Zn^{2+}$-WT complexed with EBP is shown in Fig. 3. These two structures superimpose with an RMSD of 0.45 Å for all heavy atoms, and 0.15 Å for the backbone atoms. In the WT-$Zn^{2+}$ active site (Fig. 1C), Asp301 coordinates one of the divalent metals and forms a hydrogen bond to the activated water molecule that presumably acts as a nucleophile during substrate hydrolysis [11,12]. His254 forms hydrogen bonds with Asp233 and Asp301 (Fig. 3). The arginine in H254R is in a position that would place it approximately 2.2 Å from the phosphonomethylene carbon atom of EBP in the wild-type complex. Arg254 is within 3.2 Å of the proposed activated hydroxide, and it forms hydrogen bonds with Asp233 and Asp301 in a similar pattern as observed with the native histidine (Figs. 1 and 2). An additional water molecule was also observed to be hydrogen bonded to the guanidinium groups of Arg254 (Figs. 2A and 3).

### *Ancillary binding site*

Unlike the WT-$Zn^{2+}$ enzyme in which EBP was located in the active site and the ancillary site [12], EBP was not observed to bind to the active site of H254R. However, EBP was observed to bind within a pocket located in the vicinity of Phe51 near the surface of the enzyme (Figs. 2C and 4). The electron density for EBP in this pocket in both monomers of the dimer in the asymmetric unit was well resolved (Fig. 2C). The binding of EBP within this site was first observed in the structure of the WT-$Cd^{2+}$ enzyme [11]. Although originally considered to be an artifact of the crystallization process, the kinetics of H254R suggest that binding of EBP to this site has a functional role in modulating catalysis.

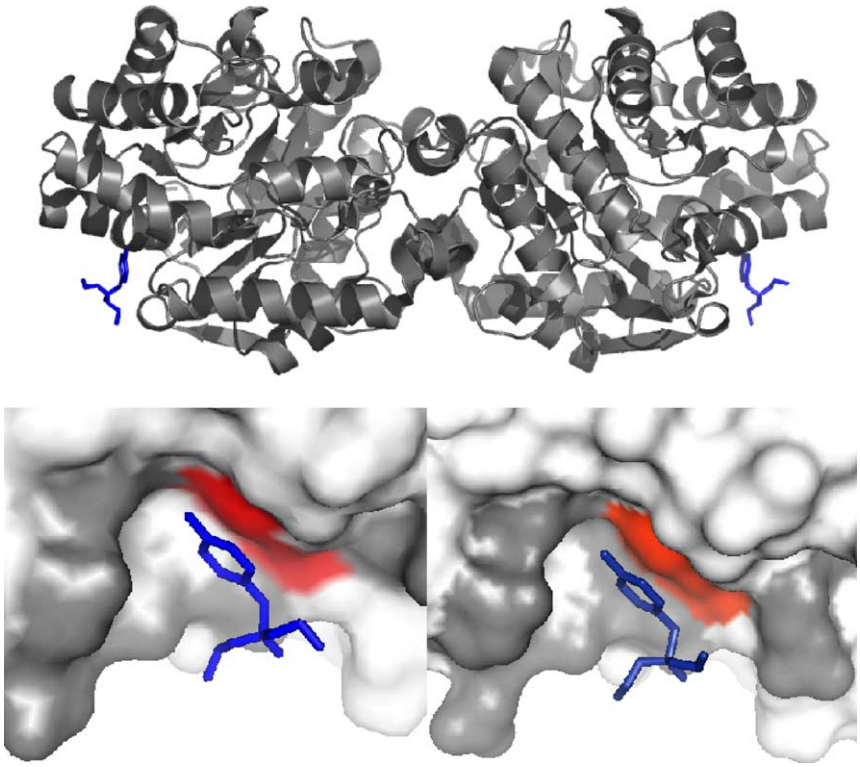

Fig. 4. Representation of the dimeric H254R structure with bound EBP (blue) in the ancillary site (top). The position of the site on the surface and the binding orientation of EBP is the same as that in the $Cd^{2+}$-liganded OPH structure [11]. Surface views (bottom) of EBP (blue) bound in the pocket of H254R (left) and in the $Cd^{2+}$-liganded structure (right). The residues forming the pocket boundaries are shaded dark gray and are essentially the same in both structures. Phe51 is colored. Figures were generated with The PyMOL Molecular Graphics System (2002) by DeLano, W.L. http://www.pymol.org. (For interpretation of the references to color in this figure legend, the reader is referred to the web version of this paper.)

*Kinetic evaluation*

Inhibition studies on the hydrolysis of paraoxon were performed using EBP as the inhibitor against the wild-type and H254R enzymes with $Co^{2+}$ as the active-site metal. Substrate saturation curves and the associated reciprocal plots for both enzymes are shown in Fig. 5. Ten different inhibitor concentrations were used in these assays, ranging from 0.4 to 6.4 mM. However, only two saturation curves, one without inhibitor and one at 6.4 mM inhibitor, are shown for clarity (Fig. 5A). EBP is an effective inhibitor of both forms of the enzyme. The H254R enzyme shows significant substrate inhibition, $K_{is} = 1.5$ mM, whereas substrate inhibition of the wild-type OPH is weak, $K_{is} = 17$ mM (Table 2). The $K_i$ values for the H254R-$Co^{2+}$ and the WT-$Co^{2+}$ enzymes, as determined via fitting the data to either Eqs. (1) or (2), were 0.25 and 0.99 mM, respectively (Table 2). The factor $\alpha$ in Eq. (2) for H254R was 20, indicating that the impact of the inhibitor was quite significant.

The nature of the inhibition of wild-type and H254R OPH by EBP was different for each enzyme, as clearly observed in the reciprocal plots in Fig. 5B. The WT-$Co^{2+}$ enzyme is competitively inhibited by EBP, whereas the H254R enzyme is inhibited in a mixed, non-competitive manner (Fig. 5B). The H254R data were best fit to a linear mixed-type of non-competitive inhibition as expressed in Eq. (2). EBP affected both the $V_{max}$ and $K_M$ in H254R. These inhibition patterns clearly indicate that the inhibitor is binding differently to the two enzymes.

*Inhibitor docking studies*

The absence of EBP in the active site of the H254R mutant enzyme prompted us to perform molecular docking studies with this inhibitor in order to gain some insight into its inability to bind to this mutant. We used the program DOCK to calculate the binding energies for the interaction of EBP with both the wild-type and H254R enzymes. DOCK generated a single orientation for EBP in the WT enzyme where all 50 of the top solutions closely superimposed onto each other (Fig. 6, right). All 50 of the top solutions had large, negative (favorable) binding energies, and their orientations were very close to the orientation of EBP bound in the active site of the wild-type enzyme as determined from the X-ray structure (Fig. 6, right).

In contrast, EBP was found to bind in remarkably different orientations when docked in the active site of the H254R mutant enzyme (Fig. 6, left). The multiple orientations indicate that there is not a single, preferred binding orientation for EBP in the H254R active site. Although the solutions generated by DOCK for EBP in the mutant active site displayed favorable, negative binding energies, they were on average weaker than those for the wild-type

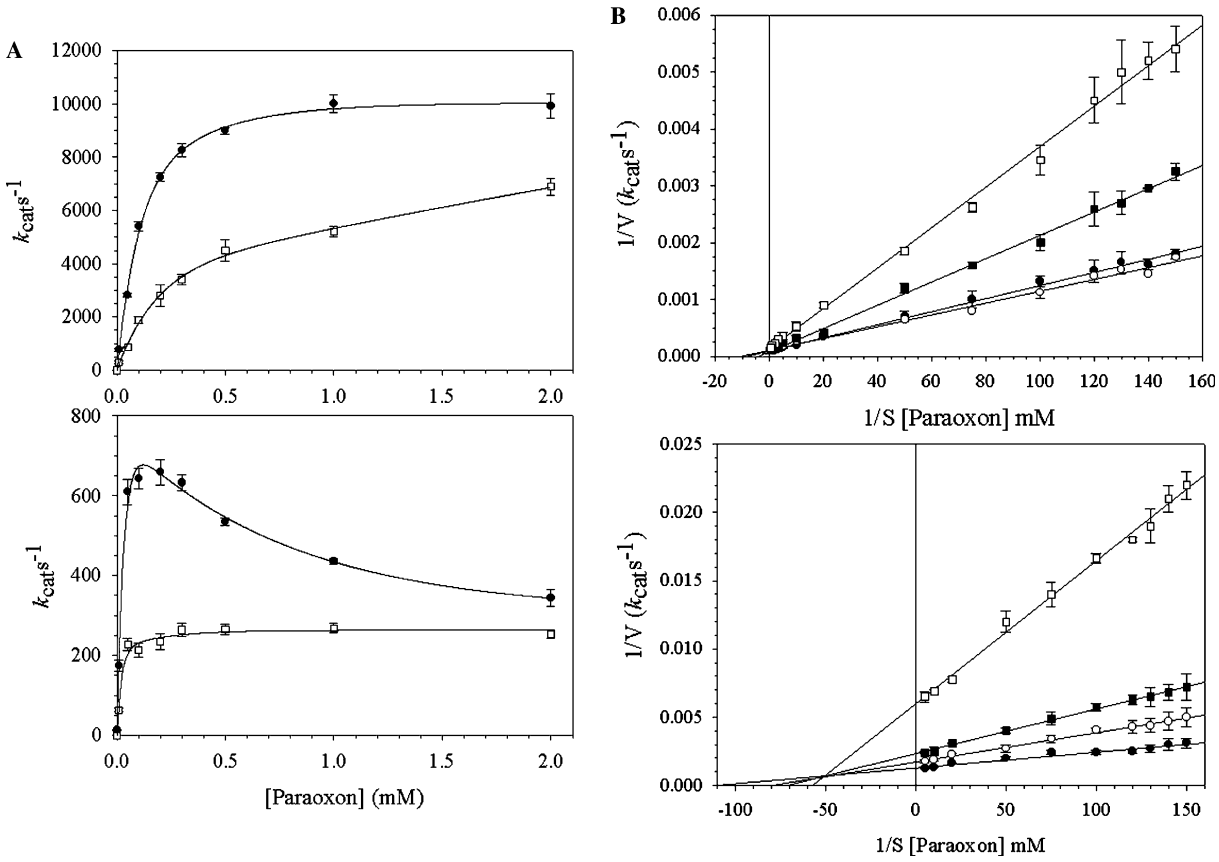


Fig. 5. (A) Substrate saturation curves for $Co^{2+}$-liganded wild-type OPH (top) and H254R (bottom). Data were fit using either Eq. (1) or Eq. (2) (see Experimental procedures). (□) 6.4 mM EBP; (●) No EBP. (B) Reciprocal plots of $Co^{2+}$-liganded wild-type OPH (top) H254R (bottom). (●) No EBP; (○) 0.4 mM EBP; (■) 1.6 mM EBP; (□) 6.4 mM EBP. For H254R, kinetic data were fit using only the lower concentrations of paraoxon (as shown).

Table 2
Kinetic constants for OPH enzymes with paraoxon[a]

| Enzyme | $k_{cat}$ ($s^{-1}$) | $K_M$ (mM) | $k_{cat}/K_M$ ($M^{-1}\,s^{-1}$) | $K_{is}$ (mM) | $K_i$ (mM) |
|---|---|---|---|---|---|
| WT-OPH | 10,500 | 0.12 | $8.75 \times 10^7$ | 17 | 0.99 |
| H254R | 750 | 0.012 | $6.25 \times 10^7$ | 1.5 | 0.25 |
| Fold-change[b] | (−)14× | (−)10× | (−)1.4× | (−)11.3× | (−)4× |

[a] $K_{is}$ and $K_i$ are the inhibition constants for paraoxon and EBP, respectively.
[b] Reflects fold increase (+) or decrease (−) in H254R values relative to those of wild-type OPH.

enzyme. This fact may suggest that although EBP can still fit into the active site of the H254R enzyme, the histidine to arginine mutation may affect the positioning and thermodynamics of ligand binding sufficiently so as to prevent it from binding to the active site.

## Discussion

The X-ray structures of OPH show that the histidines at positions 254 and 257 are not primary metal-coordinating or substrate-binding ligands. However, both of these residues directly support catalysis by participating in an extensive series of interactions with other residues within the active site. These interactions sustain and/or support the OPH-catalyzed reaction and indirectly define the structural characteristics affecting the substrate-binding site. H254R showed a 4-fold improvement in the catalytic efficiency ($k_{cat}/K_M$) for demeton-S, an analog for VX, primarily due to an increase in the turnover number ($k_{cat}$). A 3-fold improvement was observed in the $k_{cat}/K_M$ value for NPPMP, an analog for soman, due to a 3-fold improvement in substrate-binding affinity. These kinetic effects demonstrated that it is possible to redefine the relative substrate specificities of OPH since the hydrolytic rates for some substrates, demeton-S and NPPMP, increased up to 14-fold while rates for paraoxon and DFP decreased by 10- to 11-fold [16].

A catalytic role for active-site arginines has been considered to be significant in several enzymes. The structure of the complex of bovine lens aminopeptidase with its inhibitor, amastatin, has revealed a possible role for arginine as an electrophilic substrate activator [37]. An electrophilic

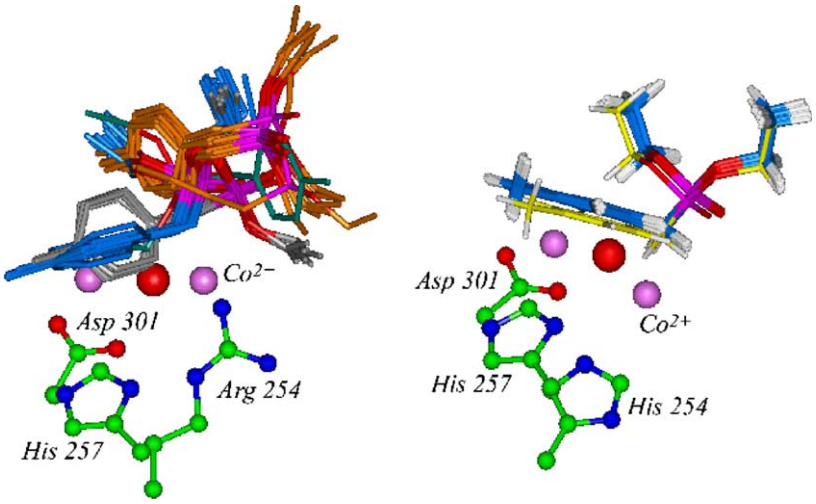


Fig. 6. Computational docking results showing the top 50 binding orientations of EBP within the active sites of H254R (left) and wild-type $Zn^{2+}$-liganded OPH [11] (right). EBP in the X-ray structure of wild-type OPH is colored yellow (right panel). (For interpretation of the references to color in this figure legend, the reader is referred to the web version of this paper.)

role for an active-site arginine has also been proposed for the mechanisms of carboxypeptidase A and thermolysin [38,39]. The catalytic influence of arginines immediately surrounding other binuclear metal centers has been documented in some protein phosphatases in which the arginine was involved in substrate recognition [40]. The important interactions for positioning the substrate, dihydroorotate, into the active site of dihydroorotase included a salt bridge with the guanidinium group of Arg20 [41]. The three-dimensional structure of H254R with a bound substrate-analog will be required to evaluate these possibilities. Interestingly, it was demonstrated previously that with demeton-S or paraoxon as a substrate, H254R requires only one equivalent of $Co^{2+}$ for catalysis suggesting that arginine in the 254 position can fulfill the role of the second $Co^{2+}$ if necessary [16]. However, H254R is still capable of tightly binding two $Co^{2+}$ atoms as indicated by the X-ray structure (Figs. 2A and 3) and kinetic studies [16,19].

Other substitutions at positions 254 and 257 in OPH were shown to alter the stereoselectivity for several organophosphate triesters [42], and directed-evolution approaches were used to enhance the degradation of chemical warfare agents and their analogs [43,44]. Those studies uncovered identical "secondary shell effects" and identified His254 and His257 as the primary amino acids that gave rise to the enhancement of catalysis. These results reinforced our "rational design" studies that preceded the directed-evolution work by 5 years. Other substitutions at 254 and 257 have altered the stereoselectivity of OPH [45] and identified these residues as important contributors to the catalytic characteristics of OPH [46], supporting our original observations.

In addition to H254 and H257, another "second shell" residue, Phe132, has been referred to as a critical residue in the 'gateway' into the active site of wild-type OPH [42]. It is positioned within the leaving group subsite and forms stacking interactions with Trp131. Modifications at Phe132 in the wild-type enzyme resulted in virtual elimination of the stereoselectivity of some substrates and appeared to affect catalysis by subtle changes in the orientation of Trp131 [42]. In the structure of H254R, the electron density associated with Phe132 indicated greater conformational freedom of this residue within both subunits (Figs. 2B and 3). Only one primary conformation of Phe132 was apparent in other OPH structures [10–12].

The three-dimensional structure of an organophosphate-degrading enzyme (OPDA) from *Agrobacterium radiobacter* has been reported [44]. OPDA and OPH share a 90% amino acid sequence identity. However, OPH has significantly higher catalytic activities and a broader substrate profile than OPDA. Nonetheless, the residues in OPDA, corresponding to His254 and His257 in OPH, are an arginine and a tyrosine, respectively. The arginine in OPDA appeared to be well placed to interact with the substrate analog, triethylphosphate, and the catalytic hydroxide, and it assumes more than one conformation in the active site [44]. A superposition of the H254R active site with that from OPDA is shown in Fig. 7, and the similarity is striking. The proximity of the arginines to the metal center and activated hydroxide in both enzymes suggests a potential catalytic role for arginine that is dependent upon the chemistry required by the various substrates for catalysis.

The presence of an ancillary-binding site on OPH capable of binding EBP has now been demonstrated for the $Co^{2+}$-substituted, H254R (this study) and the $Cd^{2+}$ and $Zn^{2+}$-substituted, wild-type OPH [11,12]. The site is visible in all existing structures of *P. diminuta* OPH [10–12,27,43,47], although the volumes of the sites vary slightly. The suggestion that this site could have a functional significance has been over-looked. In fact, it can function as an allosteric site based on our kinetic and structural data.

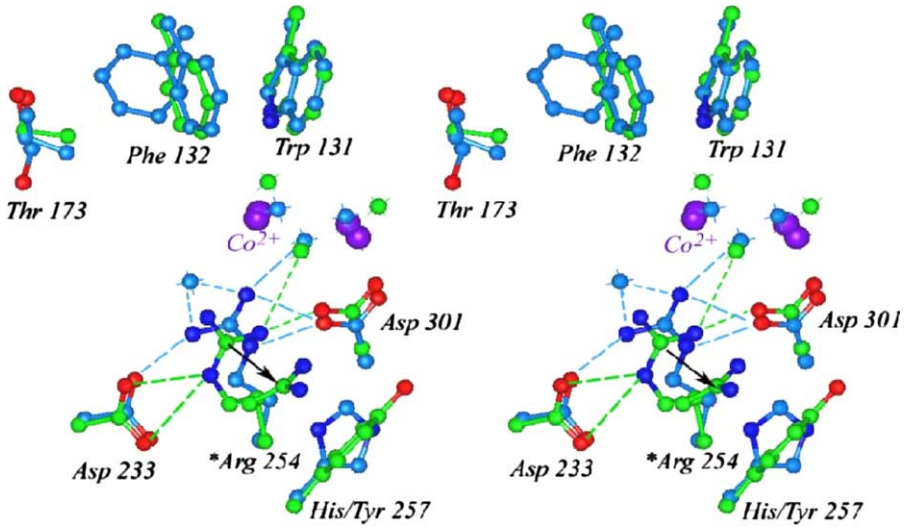


Fig. 7. Stereoview of the superposition of H254R (blue) and OPDA (green) active sites with the water molecules colored accordingly. The active-site cobalt ions are represented as purple balls. Hydrogen bonds between atoms are represented with dashed lines. The black arrow indicates the two alternate conformations for Arg254 that were present in the OPDA structure [44]. (For interpretation of the references to color in this figure legend, the reader is referred to the web version of this paper.)

It is not uncommon to see adventitious binding of various ligands present in crystallization buffers to cavities or surface pockets in a protein and these "artifacts" have provided an important source of information about unanticipated allosteric sites [48]. For example, a novel allosteric site in protein tyrosine phosphatase 1B (PTP1B) was recently discovered to bind small molecules allowing an opportunity to avoid troubles associated with inhibitors of the catalytic site [49]. Allosteric inhibition in PTP1B is a promising, new strategy for treatment of obesity and type II diabetes [49]. Similarly, an analysis of the structure of glycogen phosphorylase b (GPb) from rabbit muscle revealed a new allosteric site situated at the dimer interface, which has proven to be of practical importance in the structure-based design of new inhibitors for treatment of diabetes [50]. A final example of the importance of ancillary allosteric sites has been discovered with caspases, which are mediators of apoptosis and the inflammatory response. These enzymes are an important class of drug targets for stroke, ischemia, and cancer. It has been difficult to find drug-like caspase inhibitors because of a strong preference for an acidic side chain and an electrophilic functionality to bind at the active site [51]; however, an allosteric site was discovered in a deep cavity 14 Å away from the active site. The binding of various ligands at the allosteric site prevents peptide binding at the active site [51]. It is clear that the discovery of new allosteric sites generates opportunities for pharmaceutical development and increases our understanding of basic biological processes.

The first indication that an allosteric site exists on OPH stemmed from our observation that the $Co^{2+}$-substituted, wild-type and H254R enzymes are subject to substrate inhibition by paraoxon (Table 2). Although substrate inhibition of wild-type OPH by paraoxon is weak ($K_{is} = 17$ mM), mutation of H254 to an arginine strengthens the binding of paraoxon to this site by approximately 11.3-fold ($K_{is} = 1.5$ mM) (Table 2). One interpretation of this data is that a weak, cryptic allosteric site exists on the OPH surface that was revealed upon mutation of a residue near the active site. However, a careful survey of the available literature on OPH revealed that this cryptic allosteric site might actually bind other compounds significantly more tightly. For instance, strong substrate inhibition of $Co^{2+}$-substituted OPH by coumaphos has been noted [44] and Yang et al. reported $K_{is}$ values of 0.094 and 0.077 mM for coumaphos inhibition of *P. diminuta* and *A. radiobacter* P230 OPH enzymes, respectively. The substrate inhibition data for paraoxon and coumaphos indicate that they are both capable of binding simultaneously to the active and allosteric sties. Since these two substrates are structurally identical with the exception that the leaving group of paraoxon is 4-nitrophenol whereas the leaving group of coumaphos is chlorferon, it suggests that these two substrates bind to the same active and allosteric sites on the enzyme.

Kinetic inhibition studies with the compound EBP, which contains a 4-methylbenzyl group in place of the 4-nitrobenzyl group of paraoxon, indicate that these compounds may all bind to the same allosteric site. EBP was found to act as a competitive inhibitor against paraoxon for the $Co^{2+}$-substituted, wild-type enzyme indicating that EBP and paraoxon compete directly for the active site (Table 2, Fig. 5B). In contrast, EBP was found to inhibit the H254R enzyme via a mixed, non-competitive mechanism as indicated in Scheme 1. In the presence of high concentrations of EBP, the substrate inhibition portion of the paraoxon saturation curve for H254R is abolished (Fig. 5A, bottom). A $V_{max}$ value of $\sim 300\ s^{-1}$ is attained for the EBP-inhibited, H254R enzyme which is approximately equal to the plateau rate value of $\sim 300\ s^{-1}$ that is achieved

by the H254R enzyme in the absence of EBP (Fig. 5B). The matching rate values for H254R at saturating (1–2 mM) paraoxon concentrations in the presence or absence of EBP support a model whereby paraoxon and EBP compete for the allosteric site, but only paraoxon is capable of binding to the active site.

Our kinetic model is supported by the X-ray structure of the H254R enzyme, which shows EBP binding only to the allosteric site in this enzyme. A similar observation was made from the X-ray structure of the WT-$Cd^{2+}$ enzyme in complex with EBP, which revealed that EBP bound only in the ancillary pocket [11]. In a subsequent study, the WT-$Zn^{2+}$ enzyme was crystallized in the presence of EBP under identical conditions to those of the WT-$Cd^{2+}$ enzyme. However, with the WT-$Zn^{2+}$ enzyme, EBP was found to bind in both the ancillary site and the active site [12]. In two subsequent X-ray structural studies, EBP was replaced in the crystallization solution with other substrate analogs and the compound 2-phenylethanol was used as an additive to aid in the crystallization process [27,47]. Surprisingly, 2-phenylethanol bound in the ancillary site in the same orientation as EBP bound in the H254R structure, and as observed in the WT-$Cd^{2+}$ enzyme. This suggests that large, substituted benzyl-like groups direct compounds to the allosteric site. Residues in contact with EBP in the H254R site can be used to define the pocket in all other structures. All contacts are hydrophobic, with Phe51 contributing the most to contact surface area (Fig. 4).

The combined kinetic and structural data on *P. diminuta* OPH indicate that the binding of various substrates and inhibitors to the active site is exquisitely sensitive to the structure of the active site. Mutation of "second-shell" amino acids or substitution of different metal cations can drastically alter the substrate specificity, and can completely deny the binding of inhibitors to the site. These observations prompted us to perform a computational docking study of EBP to the active sites of wild-type and H254R mutant OPH enzymes so that we may gain insight into just how sensitive this site is to amino acid substitution. Computational modeling of the inhibitor into the active site of H254R indicated that the inhibitor EBP is able to assume multiple binding orientations within the active site albeit at lower calculated binding energies than with the wild-type enzyme (Fig. 6, left panel). In contrast, the modeled orientation of the inhibitor in the wild-type $Co^{2+}$-substituted enzyme corresponded closely to its orientation in the X-ray structure of the $Zn^{2+}$-substituted enzyme. This suggests that the mutational substitution negatively affected the precise binding of the inhibitor in the active site, and resulted in a more dynamic structure. Small changes in orientation of substrates have been shown to have large consequences on binding and catalysis of enzymes [52].

In summary, the kinetic and structural data indicate that a functional, allosteric-binding site has been identified in *P. diminuta* OPH and suggest it also exists with the *A. radiobacter* P230 enzyme as well [44]. These data, more importantly, indicate that this site is not a structural artifact. EBP was shown to associate with this allosteric-binding site and to influence catalysis in H254R but not in the native enzyme. Although this allosteric site is seemingly cryptic for the wild-type enzyme, the kinetic studies with coumaphos as the substrate indicate that this site is highly functional in the wild-type enzyme as well, and depends on the substrate under investigation [44]. Our results and observations will serve as a basis for future structural and kinetic investigations of OPH and its allosteric site, and emphasize the importance of combining X-ray structural analysis with carefully performed and detailed kinetic investigations.

Recent events have emphasized the threat from chemical and biological warfare agents. The biocatalytic destruction of chemical warfare agents has become an important area of study, and the specificity and high catalytic rates of OPH make it suitable for detoxification of nerve agent stockpiles, counteracting nerve agent attacks, and remediation of organophosphate spills [54]. The presence of an allosteric site on OPH has the potential to trap alternate states of the enzyme through binding of different ligands to the allosteric site, and to impose altered catalytic characteristics independent of the active site. Alternatively, it may be possible to enhance the long-term stability of the enzyme for use in harsh environmental conditions for the protection of military and civilian personnel.

## Acknowledgments

We thank Thomas Holton for collection of an original dataset, C. David Armstrong for help with figures, and Dr. Melinda E. Wales for many helpful discussions and critique of the manuscript.

## References

[1] C.S. McDaniel, L.L. Harper, J.R. Wild, J. Bacteriol. 170 (1988) 2306–2311.
[2] W.W. Mulbry, J.S. Karns, J. Bacteriol. 171 (1989) 6740–6746.
[3] C.M. Serdar, D.T. Gibson, Bio/Technology 3 (1985) 567–571.
[4] D.P. Dumas, J.R. Wild, F.M. Raushel, Biotechnol. Appl. Biochem. 11 (1989) 235–243.
[5] D.P. Dumas, H.D. Durst, W.F. Landis, F.M. Raushel, J.R. Wild, Arch. Biochem. Biophys. 277 (1990) 155–159.
[6] J.E. Kolakowski, J.J. DeFrank, S.P. Harvey, L.L. Szafraniec, W.T. Beaudry, K. Lai, J.R. Wild, Biocatal. Biotransform. 15 (1997) 297–312.
[7] F.C.G. Hoskin, J.E. Walker, Bull. Environ. Contam. Toxicol. 59 (1997) 9–13.
[8] V.K. Rastogi, J.J. DeFrank, T.-C. Cheng, J.R. Wild, Biochem. Biophys. Res. Commun. 241 (1997) 294–296.
[9] L. Raveh, Y. Segall, H. Leader, N. Rothschild, D. Levanon, Y. Henis, Y. Ashani, Biochem. Pharmacol. 44 (2) (1992) 397–400.
[10] M.M. Benning, J.M. Kuo, F.M. Raushel, H.M. Holden, Biochemistry 33 (1994) 15001–15007.
[11] M.M. Benning, J.M. Kuo, F.M. Raushel, H.M. Holden, Biochemistry 34 (1995) 7973–7978.
[12] J.L. VanHooke, M.M. Benning, F.M. Raushel, H.M. Holden, Biochemistry 35 (1996) 6020–6025.
[13] G.A. Omburo, J.M. Kuo, L.S. Mullins, F.M. Raushel, J. Biol. Chem. 267 (1992) 13278–13283.

[14] J.M. Kuo, M.Y. Chae, F.M. Raushel, Biochemistry 36 (1997) 1982–1988.
[15] V.E. Lewis, W.J. Donarski, J.R. Wild, F.M. Raushel, Biochemistry 27 (1988) 1591–1597.
[16] B. diSioudi, J.K. Grimsley, K. Lai, J.R. Wild, Biochemistry 38 (1999) 2866–2872.
[17] K. Lai, K.I. Dave, J.R. Wild, L.L. Szafraniec, W.T. Beaudry, S.P. Harvey, in: S.P. Harvey (Ed.), The Proceedings of 1993 U.S. Army ERDEC Scientific Conference on Chemical Defense Research, U.S. Army ERDEC, Aberdeen Proving Ground, MD, 1993, pp. 887–893.
[18] K. Lai, K.I. Dave, J.R. Wild, J. Biol. Chem. 269 (1994) 16579–16584.
[19] K. Lai, Ph.D. dissertation, Texas A&M University, College Station, TX, 1994.
[20] K. Lai, N.J. Stolowich, J.R. Wild, Arch. Biochem. Biophys. 318 (1995) 59–64.
[21] J.K. Grimsley, J.M. Scholtz, C.N. Pace, J.R. Wild, Biochemistry 36 (1997) 14366–14374.
[22] A. McPherson, Crystallization of Biological Molecules, Cold Spring Harbor Laboratory Press, Cold Spring Harbor, NY, 1999, pp. 188–192.
[23] Z. Otwinowski, W. Minor, Methods Enzymol. 276 (1997) 307–326.
[24] C.R. Kissinger, D.K. Gehlhaar, D.B. Fogel, Acta Crystallogr. D Biol. Crystallogr. 55 (Pt. 2) (1999) 484–491.
[25] A.T. Brunger, P.D. Adams, G.M. Clore, W.L. DeLano, P. Gros, R.W. Grosse-Kunstleve, J.S. Jiang, J. Kuszewski, M. Nilges, N.S. Pannu, R.J. Read, L.M. Rice, T. Simonson, G.L. Warren, Acta Crystallogr. D Biol. Crystallogr. 54 (Pt. 5) (1998) 905–921.
[26] T.A. Jones, J.Y. Zou, S.W. Cowan, M. Kjeldgaard, Acta Crystallogr. A 47 (Pt. 2) (1991) 110–119.
[27] M.M. Benning, H. Shim, F.M. Raushel, H.M. Holden, Biochemistry 40 (2001) 2712–2722.
[28] S.C. Lovell, I.W. Davis, W.B. Arendall 3rd, P.I. de Bakker, J.M. Word, M.G. Prisant, J.S. Richardson, D.C. Richardson, Proteins 50 (2003) 437–450.
[29] R.A. Laskowski, J.A. Rullmannn, M.W. MacArthur, R. Kaptein, J.M. Thornton, J. Biomol. NMR 8 (1996) 477–486.
[30] G. Vriend, J. Mol. Graph. 8 (1990) 52–56.
[31] H.M. Berman, J. Westbrook, Z. Feng, G. Gilliland, T.N. Bhat, H. Weissig, I.N. Shindyalov, P.E. Bourne, Nucleic Acids Res. 28 (2000) 235–242.
[32] T.J.A. Ewing, I.D. Kuntz, J. Comput. Chem. 18 (1997) 1175–1189.
[33] S.J. Weiner, P.A. Kollman, D.A. Case, U.C. Singh, C. Ghio, G. Alagona, G.S. Profeta Jr., P. Weiner, J. Am. Chem. Soc. 106 (1984) 765–784.
[34] S.J. Weiner, P.A. Kollman, D.T. Nguyen, D.A. Case, J. Comput. Chem. 7 (2) (1986) 230–252.
[35] M.L. Connolly, Science 221 (4612) (1983) 709–713.
[36] I.H. Segel, Enzyme Kinetics, Wiley, New York, 1975, pp. 161–226.
[37] H. Kim, H.W.N. Lipscomb, Biochemistry 32 (1993) 8465–8478.
[38] D.W. Cristianson, W.N. Lipscomb, Acc. Chem. Res. 22 (1989) 62–66.
[39] B.W. Matthews, Acc. Chem. Res. 21 (1988) 333–340.
[40] A. Mondragon, E.C. Griffith, L. Sun, F. Xiong, C. Armstrong, J.O. Liu, Biochemistry 36 (1997) 4934–4942.
[41] J.B. Thoden, G.N. Phillips Jr., T.M. Neal, F.M. Raushel, H.M. Holden, Biochemistry 40 (2001) 6989–6997.
[42] M. Chen-Goodspeed, M.A. Sogorb, F. Wu, S.-B. Hong, F.M. Raushel, Biochemistry 40 (2001) 1325–1331.
[43] C.M. Hill, W.-S. Li, J.B. Thoden, H.M. Holden, F.M. Raushel, J. Am. Chem. Soc. 125 (2003) 8990–8991.
[44] H. Yang, P.D. Carr, S.Y. McLoughlin, J.W. Liu, I. Horne, X. Qiu, C.M.J. Jeffries, R.J. Russell, J.G. Oakeshott, D.L. Ollis, Protein Eng. 16 (2003) 135–145.
[45] M. Chen-Goodspeed, M.A. Sogorb, F. Wu, F.M. Raushel, Biochemistry 40 (2001) 1332–1339.
[46] S.-B. Hong, F.M. Raushel, Methods Enzymol. 388 (2004) 256–266.
[47] M.M. Benning, S.-B. Hong, F.M. Raushel, H.M. Holden, J. Biol. Chem. 275 (2000) 30556–30560.
[48] J.A. Hardy, J.A. Wells, Curr. Opin. Struct. Biol. 14 (2004) 706–715.
[49] C. Wiesmann, K.J. Barr, J. Kung, J. Zhu, D.A. Erlanson, W. Shen, B.J. Fahr, M. Zhong, L. Taylor, M. Randal, R.S. McDowell, S.K. Hansen, Nat. Struct. Mol. Biol. 11 (6) (2004) 730–737.
[50] N.G. Oikonomakos, V.T. Skamnaki, K.E. Tsitsanou, N.G. Gavalas, L.N. Johnson, Structure 8 (6) (2000) 575–584.
[51] J.A. Hardy, J. Lam, J.R. Nguyen, T. O'Brien, J.A. Wells, Proc. Natl. Acad. Sci. USA 101 (34) (2004) 12461–12466.
[52] A.D. Mesecar, B.L. Stoddard, D.E. Koshland Jr., Science 277 (1997) 202–206.
[53] J.A. Christopher, SPOCK: The Structural Properties Observation and Calculation Kit (Program Manual), The Center for Macromolecular Design, Texas A&M University College Station, TX, 1998.
[54] A.J. Russell, J.A. Berberich, G.F. Drevon, R.R. Koepsel, Annu. Rev. Biomed. Eng. 5 (2003) 1–27.